







# Magnetic fields and outflows in the large Bok globule CB 54

Kate Pattle <sup>1,2</sup>★ Shih-Ping Lai <sup>3,4</sup> Sarah Sadavoy <sup>5</sup> Simon Coudé <sup>6</sup> Sebastian Wolf <sup>7</sup>  
Ray Furuya <sup>8</sup> Woojin Kwon <sup>9,10</sup> Chang Won Lee <sup>11,12</sup> and Niko Zielinski <sup>7</sup>

<sup>1</sup>Department of Physics and Astronomy, University College London, Gower Street, London WC1E 6BT, UK

<sup>2</sup>Centre for Astronomy, Department of Physics, National University of Ireland Galway, University Road, Galway H91 TK33, Ireland

<sup>3</sup>Institute of Astronomy and Department of Physics, National Tsing Hua University, No. 101, Section 2, Guangfu Road, Hsinchu 30013, Taiwan

<sup>4</sup>Academia Sinica Institute of Astronomy and Astrophysics, No. 1, Section 4., Roosevelt Road, Taipei 10617, Taiwan

<sup>5</sup>Department for Physics, Engineering Physics and Astrophysics, Queen's University, Kingston, ON, K7L 3N6, Canada

<sup>6</sup>SOFIA Science Center, Universities Space Research Association, NASA Ames Research Center, Moffett Field, California 94035, USA

<sup>7</sup>Institut für Theoretische Physik und Astrophysik, Christian-Albrechts-Universität zu Kiel, Leibnizstr. 15, D-24118 Kiel, Germany

<sup>8</sup>Institute of Liberal Arts and Sciences, Tokushima University, Minami Jousanajima-machi 1-1, Tokushima 770-8502, Japan

<sup>9</sup>Department of Earth Science Education, Seoul National University, 1 Gwanak-ro, Gwanak-gu, Seoul 08826, Republic of Korea

<sup>10</sup>SNU Astronomy Research Center, Seoul National University, 1 Gwanak-ro, Gwanak-gu, Seoul 08826, Republic of Korea

<sup>11</sup>Korea Astronomy and Space Science Institute, 776 Daedeokdae-ro, Yuseong-gu, Daejeon 34055, Republic of Korea

<sup>12</sup>University of Science and Technology, Korea, 217 Gajeong-ro, Yuseong-gu, Daejeon 34113, Republic of Korea

Accepted 2022 May 12. Received 2022 May 11; in original form 2022 January 31

## ABSTRACT

We have observed the large Bok globule CB 54 in 850- $\mu\text{m}$  polarized light using the POL-2 polarimeter on the James Clerk Maxwell Telescope (JCMT). We find that the magnetic field in the periphery of the globule shows a significant, ordered deviation from the mean-field direction in the globule centre. This deviation appears to correspond with the extended but relatively weak <sup>12</sup>CO outflow emanating from the Class 0 sources at the centre of the globule. Energetics analysis suggests that if the outflow is reshaping the magnetic field in the globule's periphery, then we can place an upper limit of  $< 27 \mu\text{G}$  on the magnetic field strength in the globule's periphery. Comparison with archival *Planck* and CARMA measurements shows that the field in the centre of the globule is consistent over several orders of magnitude in size scale, and oriented parallel to the density structure in the region in projection. We thus hypothesize that while non-thermal motions in the region may be sub-Alfvénic, the magnetic field is subdominant to gravity over a wide range of size scales. Our results suggest that even a relatively weak outflow may be able to significantly reshape magnetic fields in star-forming regions on scales  $> 0.1 \text{ pc}$ .

**Key words:** stars: formation – ISM: individual objects: CB 54 – ISM: magnetic fields – submillimetre: ISM.

## 1 INTRODUCTION

Outflows from protostellar systems play an important role in the dynamics of the molecular clouds from which they form, providing instantaneous feedback on the cloud as they eject angular momentum and kinetic energy from the forming stellar system (Bally 2016). Molecular clouds, like the lower density interstellar medium (ISM), are threaded by magnetic fields on all size scales (e.g. Crutcher 2012). Outflows and magnetic fields in combination may play a significant role in setting the star formation efficiency (SFE) of both cores (e.g. Offner & Chaban 2017) and clouds (e.g. Krumholz & Federrath 2019).

Interferometric observations of large samples of protostellar sources have found that magnetic fields and outflows are typically randomly aligned, with the possibility of a well-aligned subset, on interferometric (1000s of au) scales (Hull et al. 2014; Hull & Zhang 2019), while a comparable single-dish study found outflows to be

misaligned with respect to magnetic fields by an average of  $50^\circ \pm 15^\circ$  in 3D, but did not rule out random orientation (Yen et al. 2021). Recent observations have shown that in some cases, dust polarization around young protostars appears to trace their outflow cavity walls, suggesting compression and rearrangement of magnetic fields by outflow feedback (Hull et al. 2020; Lyo et al. 2021). However, the physical scales over which and time-scales on which this rearrangement can occur are not well-established, and neither is the range of magnetic environments in which this rearrangement of the field can take place.

Bok globules (Bok & Reilly 1947) are isolated clumps of molecular gas, typically containing a few tens of solar masses within a diameter of a few tenths of a parsec (Launhardt et al. 2010). They are therefore a relatively simple environment in which the low-mass star formation process can be studied.

CB 54 (Clemens & Barvainis 1988), also known as LBN 1042 (Lynds 1965), is a large ( $\sim 0.5 \text{ pc}$  diameter) globule at a distance of  $\sim 1.5 \text{ kpc}$  which is associated with the Vela OB1 complex (Ciardi & Gómez Martín 2007; Sen et al. 2021). CB 54 is an example of a forming group of low-mass stars (Ciardi & Gómez Martín 2007),

\* E-mail: [k.pattle@ucl.ac.uk](mailto:k.pattle@ucl.ac.uk)

and so whether it should be described as a Bok globule or as a small cloud is arguable. As the maximum mass of a Bok globule is not well defined, and as CB 54 is an isolated, apparently spheroidal cloud (approximately circular in projection) and is consistently referred to as a Bok globule in the literature, we continue to define it as such in this work.

CB 54 contains five known point sources: the NIR-bright sources CB54YC1-I and -II (Yun 1996), and the deeply embedded sources MIR-a, -b, and -c (Ciardi & Gómez Martín 2007). CB54YC1-II is established as a Class I source (Yun 1996); the classification of CB54YC1-I is more uncertain, with possibilities including its being a highly extinguished embedded A or B star, a background G or F giant, or a very highly inclined embedded protostar (Ciardi & Gómez Martín 2007). The three remaining sources, MIR-a, -b and -c, are deeply embedded Class 0 sources forming in close proximity to one another (Ciardi & Gómez Martín 2007), coincident with the IRAS source PSC 07020-1618 and with a peak in submillimetre emission (Launhardt et al. 2010). At least one of these sources is driving a small-scale molecular outflow oriented  $108^\circ$  E of N (Hull et al. 2014). A larger scale outflow from CB 54, oriented broadly NE/SW ( $\sim 45^\circ$  E of N), was mapped by Yun & Clemens (1994). Sepúlveda et al. (2011) suggest that this large-scale outflow is also excited by one or more of the Class 0 sources.

Using measurements of polarized extinction of background starlight, Sen et al. (2005) found a mean magnetic field direction in CB 54 of  $116^\circ \pm 38^\circ$  E of N. Bertrang, Wolf & Das (2014) found a complex geometry, with near-infrared (NIR) extinction polarization vectors on the northern side of the globule broadly aligned with the Yun & Clemens (1994) CO outflow axis. However, Sen et al. (2021), using *R*-band extinction polarization, find a random distribution of polarization angles, suggesting significant amounts of foreground extinction. Henning et al. (2001) observed CB 54 in 850- $\mu\text{m}$  polarized emission with the SCUPOL polarimeter on the James Clerk Maxwell Telescope (JCMT), finding a somewhat random distribution of polarization vectors. Wolf, Launhardt & Henning (2003) re-analysed these data, and found a weak correlation between the magnetic field and large-scale outflow directions in CB 54.

In this paper, we present JCMT 850- $\mu\text{m}$  observations of CB 54, made in polarized light using the POL-2 polarimeter. We describe our observations and the data reduction process in Section 2. In Section 3, we discuss the magnetic field geometry, mass and density properties and energetic balance of the globule, and make comparison to previous observations of the globule. In Section 4, we discuss our results. Section 5 summarizes this work.

## 2 OBSERVATIONS

We observed the Bok globule CB 54 15 times between 2019 March 3 and 2021 February 26 using the POL-2 polarimeter (Friberg et al. 2016) mounted on the Submillimetre Common-User Bolometer Array 2 (SCUBA-2; Holland et al. 2013) on the JCMT. The data were taken in Band 2 weather ( $0.05 < \tau_{225\text{ GHz}} < 0.08$ ) under project codes M19AP016, M20AP022, and M21AP028. Each observation consisted of a 42-min POL-2-DAISY scan pattern.

The data were reduced using the *pol2map*<sup>1</sup> script recently added to the SMURF package in the *Starlink* software suite (Chapin et al. 2013). See Pattle et al. (2021b) for a detailed description of the current POL-2 data reduction process. Instrumental polarization (IP)

was corrected for using the ‘August 2019’ IP model.<sup>2</sup> The 850- $\mu\text{m}$  data were calibrated using a flux conversion factor (FCF) of 2795 mJy arcsec<sup>-2</sup> pW<sup>-1</sup> using the post-2018 June 30 SCUBA-2 FCF of 2070 mJy arcsec<sup>-2</sup> pW<sup>-1</sup> (Mairs et al. 2021) multiplied by a factor of 1.35 to account for additional losses in POL-2 (Friberg et al. 2016). POL-2 observes simultaneously at 850 and 450  $\mu\text{m}$ , but we consider only the 850- $\mu\text{m}$  observations in this work as the 450- $\mu\text{m}$  data reduction process remains under development.

We binned our output vector catalogue to 8-arcsec (approximately Nyquist-sampled) pixels. The per-pixel RMS noise values in the vector catalogue were then remodelled using the *pol2noise* script, which models map variance as the sum of three components, based on exposure time, the presence of bright sources, and residuals. The average RMS noise in Stokes *Q* and *U* and *I* in the central 3 arcmin of the map on 8-arcsec pixels is 0.004 mJy arcsec<sup>-2</sup> (1.0 mJy beam<sup>-1</sup>).

The observed polarized intensity is given by

$$PI' = \sqrt{Q^2 + U^2}. \quad (1)$$

We debiased this quantity using the modified asymptotic estimator (Plaszczynski et al. 2014; Montier et al. 2015):

$$PI = PI' - \frac{1}{2} \frac{\sigma^2}{PI'} \left( 1 - e^{-\left(\frac{PI'}{\sigma}\right)^2} \right), \quad (2)$$

where  $\sigma^2$  is the weighted mean of the variances  $\sigma_Q^2$  and  $\sigma_U^2$ ,

$$\sigma^2 = \frac{Q^2 \sigma_Q^2 + U^2 \sigma_U^2}{Q^2 + U^2}, \quad (3)$$

calculated on a pixel-by-pixel basis. Debiased polarization fraction is given by  $p = PI/PI'$ .

Polarization angle is given by

$$\theta_p = 0.5 \arctan(U, Q). \quad (4)$$

We note that the polarization angles which we detect are not true vectors, as they occupy a range in angle  $0^\circ$ – $180^\circ$ . We none the less refer to our measurements as vectors for convenience, in keeping with the general convention in the field.

Throughout this work, we assume that dust grains are aligned with their major axis perpendicular to the magnetic field direction (e.g. Andersson, Lazarian & Vaillancourt 2015), and so that the plane-of-sky magnetic field direction can be inferred by rotating  $\theta_p$  by  $90^\circ$ .

## 3 RESULTS

850- $\mu\text{m}$  polarization and magnetic field vector maps are shown in Fig. 1. In these figures and throughout the following analysis, we use the vector selection criteria  $p/\delta p > 3$  and  $I/\delta I > 5$ . Note that  $p/\delta p > 3$  is equivalent to  $\delta\theta_p < 9^\circ$  (cf. Serkowski 1962). Maps of Stokes *Q* and *U* emission, and of *PI'*, are shown in Appendix A.

### 3.1 Magnetic field geometry

The six vectors which we detect in the dense centre of CB 54 are quite uniform, with a mean position angle  $\theta_B = 163^\circ \pm 8^\circ$ . However, in the periphery of the globule, the magnetic field geometry appears curved, showing well-ordered deviation from the field direction which we measure in the centre of the globule. The field in the periphery of

<sup>1</sup><http://starlink.eao.hawaii.edu/docs/sun258.htx/sun258ss73.html>

<sup>2</sup><https://www.eaoobservatory.org/jcmt/2019/08/new-ip-models-for-pol2-data/>

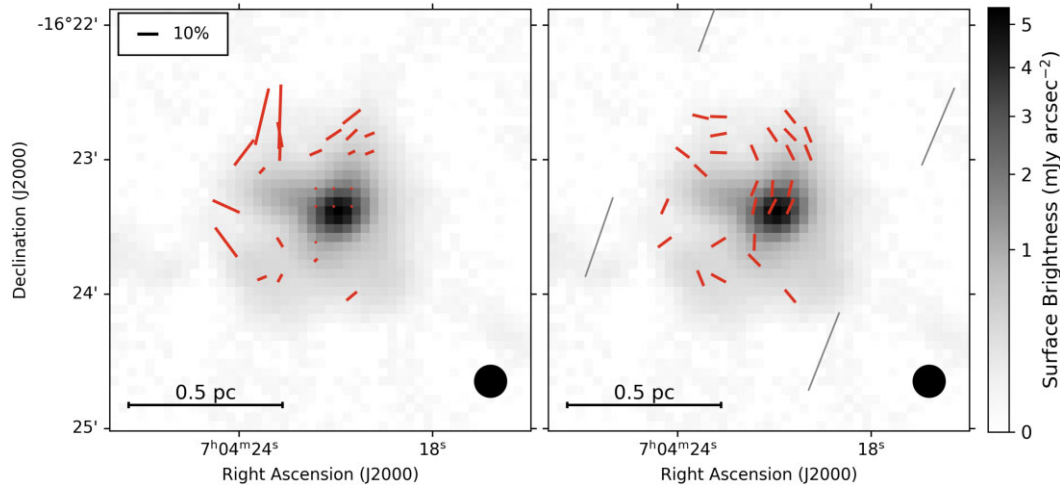


**Figure 1.** Our observations of CB 54. Left-hand panel shows polarization vectors ( $I/I > 5$ ,  $p/dp > 3$ ), scaled by polarization fraction. Right-hand panel shows uniform-length magnetic field vectors (polarization vectors rotated by  $90^\circ$ ). Red vectors are POL-2 measurements; grey vectors are *Planck* measurements which, with an effective resolution of 15 arcmin, are significantly oversampled. The background image is POL-2 850- $\mu\text{m}$  Stokes  $I$  emission. The JCMT beam size is shown in the lower right-hand of each panel.

the globule has a mean position angle of  $67^\circ \pm 45^\circ$ , and a median position angle of  $47^\circ$ .

We compared our POL-2 data to *Planck* 353-GHz dust polarization maps of CB 54 (Planck Collaboration XIX 2015; Planck Collaboration XLVIII 2016). The *Planck* archive measures polarization angle relative to Galactic north, and uses the convention  $\theta_p = 0.5 \arctan(-U, Q)$ . We calculated the difference in polarization angle between galactic and equatorial systems,  $\psi$ , using the relation

$$\begin{aligned} \psi &= \theta_{p,\text{gal}} - \theta_{p,\text{eq}} \\ &= \arctan\left(\frac{\cos(l - 32:9)}{\cos b \cot 62:9 - \sin b \sin(l - 32:9)}\right) \end{aligned} \quad (5)$$

(Corradi, Aznar & Mampaso 1998). For  $(l, b) = (228:99, -4:62)$ ,  $\psi = -63:08$ .

*Planck* observations of CB 54 are shown in Fig. 2. We used the GNLIC foreground dust model (Planck Collaboration XLVIII 2016), as it provides covariance matrices for each Stokes parameter, but the Commander dust model (Planck Collaboration XIX 2015) produces near-identical polarization angles in CB 54. The mean-field direction in the *Planck* data is  $158^\circ \pm 7^\circ$  E of N, consistent with the value of  $163^\circ \pm 8^\circ$  that we measure in the densest part of the globule with POL-2. Both of these values are also consistent within uncertainties with the mean-field direction of  $116^\circ \pm 38^\circ$  measured in the region by Sen et al. (2005).

Although the magnetic field which we observe in the centre of CB 54 is well-ordered and consistent with the *Planck*-scale field, the magnetic field direction in the periphery of the globule deviates significantly from that seen in the centre. There is a striking similarity between the magnetic field morphology in the periphery of CB 54 and the contours of the outflow described by Yun & Clemens (1994), as shown in Fig. 3. This is most apparent in the northern (red) wing of the outflow, as more polarized emission, is detected on the north-eastern side of the globule, and is consistent with previous NIR extinction polarization measurements on larger scales (Bertrang et al. 2014). The few vectors which we detect on the south-western side of the globule are also broadly aligned with the blue wing of the outflow.

On the eastern periphery of the globule, away from the outflow, there are a small number of POL-2 vectors which appear broadly aligned with the *Planck*-scale field.

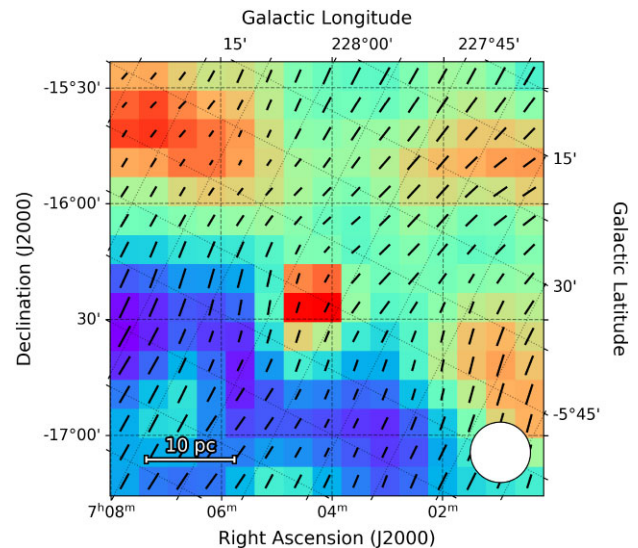


**Figure 2.** *Planck* magnetic field vectors in CB 54, using the GNLIC foreground dust model (Planck Collaboration XIX 2016). Vector length is proportional to polarization fraction. All *Planck* vectors shown have  $p/dp > 3$ . Dashed grid lines show equatorial projection; dotted grid lines show galactic projection. The effective resolution of this data set is 15 arcmin, and the pixels are Nyquist sampled. The beam is shown in the lower right-hand corner.

### 3.2 Comparison with SCUPOL

We compared our POL-2 data with previous measurements of 850- $\mu\text{m}$  polarization in CB 54, made using the SCUPOL polarimeter. These data were originally presented by Henning et al. (2001). We use the updated reduction presented by Matthews et al. (2009) in the SCUPOL Legacy Catalogue. These data are presented on 10 arcsec pixels. We selected SCUPOL vectors using the criteria  $I/I > 5$ ,  $p/dp > 3$  and  $dp < 4$  per cent (cf. Matthews et al. 2009). The SCUPOL and POL-2 vectors are compared in Fig. 4. The two sets of polarization angles are similar: in the centre of CB 54, they agree well, with the mean magnetic field angle over the five central SCUPOL vectors

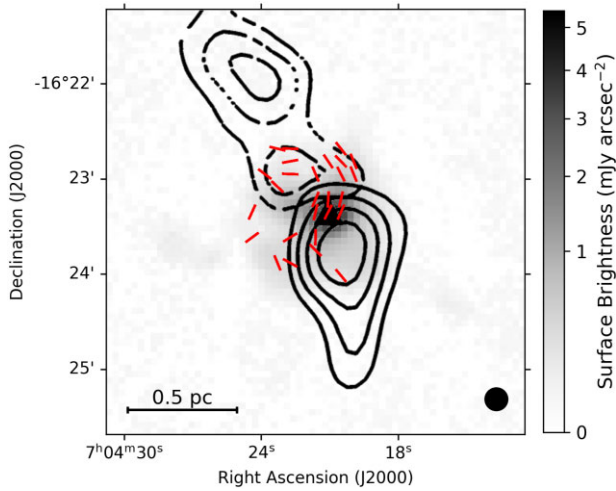


**Figure 3.** The large-scale  $^{12}\text{CO}$  outflow mapped by Yun & Clemens (1994), overlaid on our POL-2 data. Note similarity between the magnetic field and outflow morphology. The southern lobe (solid contours) is blue-shifted emission ( $13\text{--}17\text{ km s}^{-1}$ ), northern lobe (broken contours) is red-shifted emission ( $23\text{--}27\text{ km s}^{-1}$ ). Background image shows POL-2 Stokes  $I$  emission.

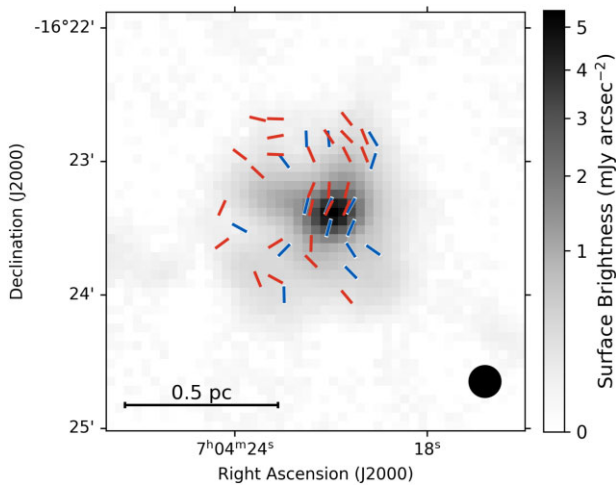


**Figure 4.** Comparison of POL-2 (red; this work) and SCUPOL (blue with white outline; Matthews et al. 2009) magnetic field vectors in CB 54. Background image shows POL-2 Stokes  $I$  emission.

being  $159^\circ \pm 6^\circ$  E of N, compared to the  $163^\circ \pm 8^\circ$  E of N which we measure with POL-2. In the periphery of the globule, the SCUPOL and POL-2 vectors show qualitative similarity, and the significant deviations from the mean direction in the globule centre are apparent in both cases. A two-sided KS test suggests that the two sets of angles are consistent with having been drawn from the same distribution, with a  $p$ -value of 0.37. Histograms of the POL-2 and SCUPOL angles are shown in Fig. 5. The SCUBA/SCUPOL and SCUBA-2/POL-2 systems are fully independent, consisting of separate polarimeters, cameras, observing modes, and data reduction algorithms.

Henning et al. (2001) inferred a plane-of-sky magnetic field strength of  $60_{-8}^{+11}\ \mu\text{G}$  in the higher density centre of CB 54 using the Davis–Chandrasekhar–Fermi (DCF; Davis 1951, Chandrasekhar & Fermi 1953) method. However, to do so they used a measured angle dispersion of  $42_{-8.0}^{+11.1}$ , significantly greater than the limit of  $\sim 25^\circ$  above which the DCF method has been found to become

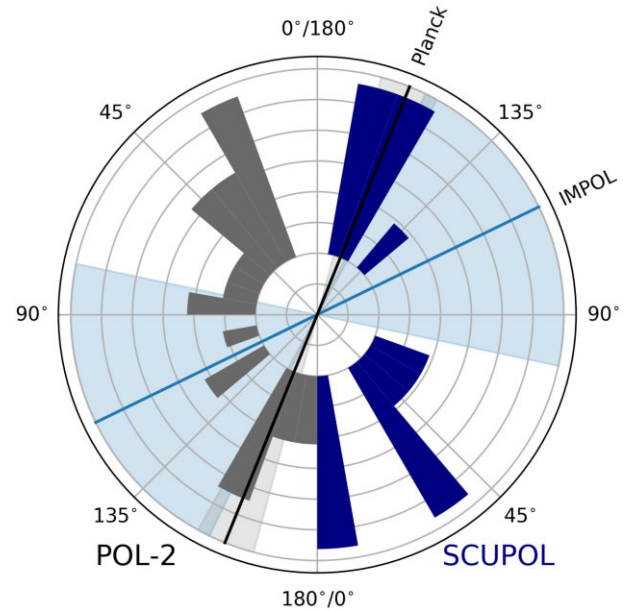


**Figure 5.** Circular histograms of POL-2 (grey) and SCUPOL (blue) magnetic field angles. Mean *Planck* and IMPOL (Sen et al. 2005) magnetic field angles across CB 54 are shown, with their uncertainties shown as shaded sectors. The POL-2 histogram is shown over the angle range  $0^\circ\text{--}180^\circ$  E of N, while the SCUPOL histogram is shown over the range  $180^\circ\text{--}360^\circ$ . Due to the  $\pm 180^\circ$  ambiguity on polarization vector measurements, this range is effectively identical to the range  $0^\circ\text{--}180^\circ$ , and so opposite angles on the plot agree. In Cartesian space, the area of each histogram is normalised to 1; the projection of the histograms on to a circle means that their areas are distorted.

unreliable (Ostriker, Stone & Gammie 2001). Wolf et al. (2003) derived the magnetic field strength in CB 54 to be  $104_{-21}^{+24}\ \mu\text{G}$ , using the same angular dispersion but a hydrogen number density of  $n(\text{H}) = 1.5 \times 10^5\ \text{cm}^{-3}$ .

### 3.3 Globule mass and density

We measured the total  $850\text{-}\mu\text{m}$  flux density in a 2 arcsec-diameter aperture centred on CB 54 to be  $4.19 \pm 0.25\ \text{Jy}$ . The uncertainty on this value is dominated by the 6 per cent SCUBA-2  $850\text{-}\mu\text{m}$  calibration uncertainty (Mairs et al. 2021).

We thus calculated the mass of CB 54 using the Hildebrand (1983) relation,

$$M = \frac{F_\nu D^2}{\kappa_\nu B_\nu(T)}, \quad (6)$$

where  $M$  is mass,  $F_\nu$  is flux density at frequency  $\nu$ ,  $D$  is distance to the source,  $\kappa_\nu$  is dust opacity, and  $B_\nu(T)$  is the *Planck* function at temperature  $T$ . Taking  $D = 1.5\ \text{kpc}$ ,  $\kappa_\nu = 0.0125\ \text{cm}^2\ \text{g}^{-1}$  (e.g. Johnstone et al. 2017) and  $T = 15\ \text{K}$  (Sepúlveda et al. 2011), this gives a mass of  $117 \pm 7\ M_\odot$  for CB 54. We have here considered only the uncertainty on  $F_\nu$ , and so the formal error bars on our measured mass are quite small.

This value for the mass of CB 54 can only be considered as an approximation.  $D$ ,  $T$ , and  $\kappa_\nu$  are all subject to significant uncertainties. We adopt a distance of 1.5 kpc to CB 54 (Launhardt & Henning 1997; Ciardi & Gómez Martín 2007); recent extinction measurements support this distance, but find a potential range of distances to the globule of 1.5–2 kpc (Sen et al. 2021).  $\kappa_\nu$  is likely to be accurate to within a factor of 2 (Ossenkopf & Henning 1994; Roy et al. 2014). Sepúlveda et al. (2011) give  $T \lesssim 15\ \text{K}$  in CB 54,

as discussed below, so taking  $T = 15$  K gives us a lower limit on the mass traced by POL-2.

We will not have traced the full extent of the dust emission from CB 54 in these observations: SCUBA-2 is insensitive to large-scale structure due to atmospheric filtering effects (Chapin et al. 2013), and POL-2 is more so due to its low scanning speed (Friberg et al. 2016). However, the angular size of CB 54 is  $\sim 2$  arcmin, smaller than the maximum allowed size scale in POL-2 observations of 5 arcmin (Friberg et al. 2016), and the source is strongly centrally peaked, so this effect may not significantly reduce the measured mass.

Conversely, we will also have some contamination from the  $^{12}\text{CO } J = 3 \rightarrow 2$  line in our Stokes  $I$  map (Drabek et al. 2012), which will contribute to the measured 850- $\mu\text{m}$  flux. This is likely to be the most significant in the outer parts of the globule, where the dust column density is low, but the net contribution of  $^{12}\text{CO } J = 3 \rightarrow 2$  to SCUBA-2 850- $\mu\text{m}$  emission in star-forming regions is typically  $< 20$  per cent (Drabek et al. 2012; Pattle et al. 2015; Coudé et al. 2016).

Our estimated mass implies an average density of molecular hydrogen over CB 54 of  $n(\text{H}_2) \sim 5.1 \times 10^3 \text{ cm}^{-3}$ , taking CB 54 to be a uniform sphere, i.e.

$$n(\text{H}_2) = \frac{3M}{4\pi\mu m_{\text{H}} r^3}, \quad (7)$$

where we take  $\mu = 2.8$  to be the mean particle mass. However, this is an average over the entire globule. The centre of the globule, in which the Class 0 protostars are located, is significantly higher density. We therefore model CB 54 as a two-layered sphere, with a high-density central core embedded in lower density surroundings. We took the inner sphere to have a radius of 16 arcsec, in order to include the high-density central region in which the magnetic field direction is uniform, and in which the protostars are embedded, and the outer sphere to have an inner radius of 16 arcsec and an outer radius of 60 arcsec.

We determined the mass and volume density of the inner and outer regions by initially considering the flux in an annular region covering gas in the outer sphere only, with an inner radius of 16 arcsec and an outer radius of 60 arcsec. The total flux in the annular region was  $2.28 \pm 0.14$  Jy. For the values of  $D$ ,  $\kappa_{\nu}$ , and  $B_{\nu}(T)$  listed above, this is equivalent to a mass of  $64 \pm 4 M_{\odot}$ . The average volume density in the annular region, and so in the ‘outer sphere’ in our model of CB 54, is thus given by

$$n(\text{H}_2) = \frac{M}{\mu m_{\text{H}}} \left( \frac{4}{3} \pi a^2 - 2\pi a^2 \sqrt{r^2 - a^2} - \frac{2}{3} \pi \left( r - \sqrt{r^2 - a^2} \right)^2 \left( 2r + \sqrt{r^2 - a^2} \right) \right)^{-1}, \quad (8)$$

where  $r = 60$  arcsec and  $a = 16$  arcsec, and so we estimate  $n(\text{H}_2) = 3.0 \times 10^3 \text{ cm}^{-3}$  in the periphery of the globule.

Conversely, the total flux in the central circular aperture, of radius 16 arcsec, is  $1.91 \pm 0.11$  Jy, equivalent to a mass of  $53 \pm 3 M_{\odot}$ . Using our previous density estimate for gas in the outer sphere, we estimate that the column of emission contained in the annulus represents the sum of contributions from  $6 M_{\odot}$  of material in the low-density outer sphere, and from  $47 M_{\odot}$  of material in the high-density inner sphere. The inner sphere thus has an average density of  $1.0 \times 10^5 \text{ cm}^{-3}$ .

These values are quite consistent with previous measurements of CB 54. Sepúlveda et al. (2011) measured a gas temperature of  $T \lesssim 15$  K, a mass of  $\gtrsim 62 M_{\odot}$ , and an average density in CB 54 of  $\sim 3.3 \times 10^3 \text{ cm}^{-3}$  from  $\text{NH}_3$  emission (a suitable dense gas tracer, with a critical density of  $\sim 2 \times 10^3 \text{ cm}^{-3}$ ; e.g. Juvella et al. 2012). The  $\text{NH}_3$  contours shown by Sepúlveda et al. (2011) correspond

well to the 850- $\mu\text{m}$  dust emission which we observe. Our value for the density in the central region is also comparable to previous measurements. Henning et al. (2001) found a density  $n(\text{H}) = 5 \times 10^4 \text{ cm}^{-3}$  within the FWHM contour of a Gaussian profile fitted to CB 54, while Wolf et al. (2003) found a density of  $1.5 \times 10^5 \text{ cm}^{-3}$ .

### 3.4 Energetics analysis

In this section, we present a crude energetics analysis to determine an approximate upper limit on the magnetic field strength in the periphery of CB 54, if the magnetic field is indeed being reshaped by the large-scale outflow.

Yun & Clemens (1994) find that the large-scale CO outflow has a mass in its blue wing of  $0.55(D/600 \text{ pc})^2 M_{\odot}$ , and in its red wing of  $0.2(d/600 \text{ pc})^2 M_{\odot}$ . They further find a total momentum of  $4.4(D/600 \text{ pc})^2 M_{\odot} \text{ km s}^{-1}$ , and an energy of  $10^{43}(d/600 \text{ pc})^2 \text{ erg}$  for the outflow. The length-scale of the outflow is 1.4 arcmin, and its dynamical time is  $2.8 \times 10^4(D/600 \text{ pc}) \text{ yr}$ . Taking the distance to CB 54 to be 1.5 kpc (Ciardi & Gómez Martín 2007; Sen et al. 2021), the total outflow mass is  $4.7 M_{\odot}$ , the energy is  $6.3 \times 10^{43} \text{ erg}$ , and the dynamical time is  $7 \times 10^4 \text{ yr}$ , while the length-scale of the outflow is 0.61 pc.

From Fig. 3, we estimate an aspect ratio in the red lobe of the outflow of  $\sim 0.5:1$ , and of  $\sim 1:1$  in the blue lobe. If we consider each lobe as a cylinder of height 0.61 pc, we estimate a total volume of the outflow of  $\sim 6.6 \times 10^{54} \text{ cm}^3$ . The estimated average energy density in the outflow is thus  $u_{\text{outflow}} \sim 1 \times 10^{-11} \text{ erg cm}^{-3}$ . Alternatively, if we consider each lobe of the outflow as a right circular cone of the same height, we estimate a volume of  $\sim 2.2 \times 10^{54} \text{ cm}^3$ , and so an average energy density of  $u_{\text{outflow}} \sim 3 \times 10^{-11} \text{ erg cm}^{-3}$ .

If the magnetic field is reshaped by the outflow, it implies that the magnetic energy density in CB 54 ( $u_{\text{B}}$ ) is less than the outflow energy density, i.e.

$$u_{\text{B}} < u_{\text{outflow}}. \quad (9)$$

Magnetic energy density,  $u_{\text{B}}$ , is given in cgs units by

$$u_{\text{B}} = \frac{B^2}{8\pi}, \quad (10)$$

where  $B$  is magnetic field strength, and so equation (9) is equivalent to placing an upper limit on  $B$ , such that

$$B < \sqrt{8\pi u_{\text{outflow}}}. \quad (11)$$

Our estimate of  $u_{\text{outflow}}$  implies  $u_{\text{B}} < 1\text{--}3 \times 10^{-11} \text{ erg cm}^{-3}$ , and so that  $B < 16 \mu\text{G}$  (cylindrical outflow geometry) or  $B < 27 \mu\text{G}$  (conical outflow geometry) in the low-density peripheral regions of CB 54 where the field appears to have been reshaped by the outflow. We therefore adopt an upper limit on the magnetic field strength in the periphery of CB 54 of  $B < 27 \mu\text{G}$ .

We note that while this upper limit is very approximate, it is relatively insensitive to the uncertainty on the distance to CB 54. If we take CB 54 to be at a distance of 1.1 kpc rather than 1.5 kpc (Brand & Blitz 1993), the upper limit on  $B$  is modified by a factor  $\sqrt{1.5/1.1} = 1.16$ , becoming  $B < 19 \mu\text{G}$  (cylindrical outflow) or  $B < 32 \mu\text{G}$  (conical outflow). Conversely, taking the upper-limit distance to CB 54 of 2 kpc (Sen et al. 2021) leads to  $B < 14 \mu\text{G}$  or  $B < 23 \mu\text{G}$ .

Crutcher et al. (2010) used archival Zeeman measurements to derive a maximum magnetic field strength as a function of gas density of

$$B_{\text{max}} = 10 \left( \frac{n(\text{H})}{300 \text{ cm}^{-3}} \right)^{0.65} \mu\text{G} \quad (12)$$

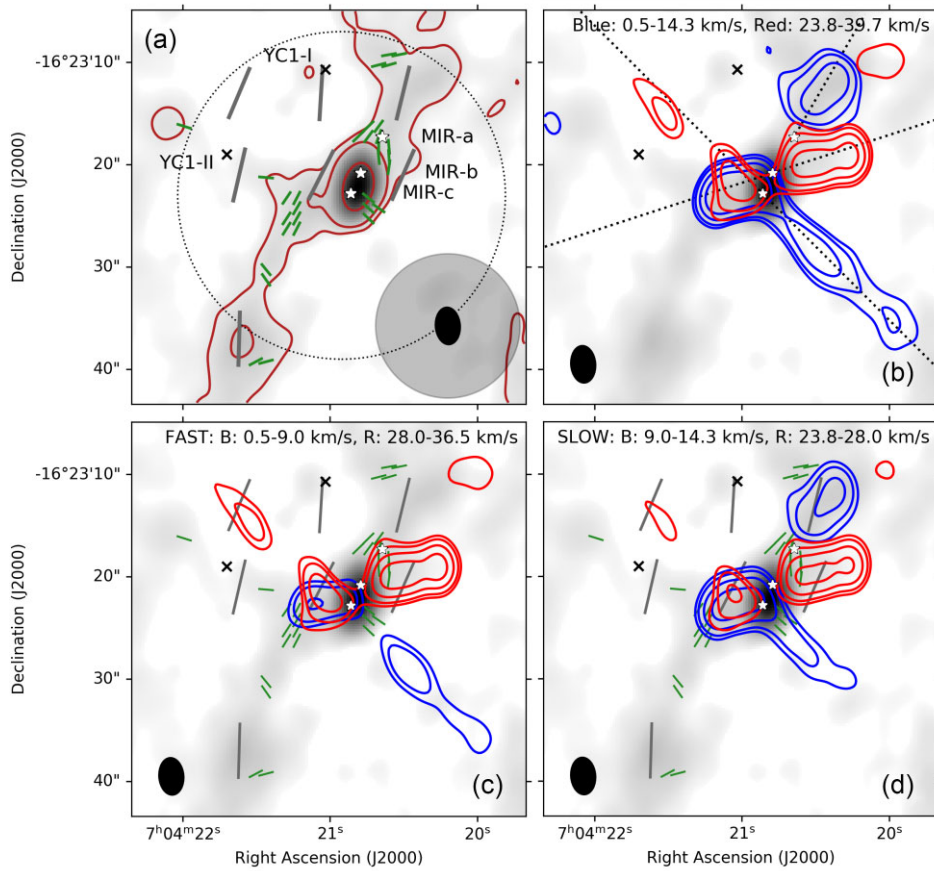


**Figure 6.** CARMA TADPOL observations of CB 54 (Hull et al. 2014). Background shows 1.3-mm dust continuum. Green vectors show magnetic field direction inferred from 1.3-mm dust polarization observations. Grey vectors show POL-2 magnetic field vectors, as presented in Fig. 1. Blue and red contours in Panels (b)–(d) show the  $^{12}\text{CO } J = 2 - 1$  transition, integrated over velocity ranges away from the systemic velocity of CB 54 (as determined by Hull et al. 2014). Contour intervals: 2, 3, 5, and  $8\sigma$ , where  $\sigma = 1.28 \text{ mJy/CARMA beam}$ . Panel (a) CARMA 1.1mm continuum, with embedded sources labelled. Maroon contours show 3, 10, and 50 percent of the maximum brightness, emphasizing the extent and direction of the ridge structure in which the protostars are embedded. Dotted circle shows the 16 arcsec-radius area over which the central density is estimated in the POL-2 data. Panel (b) contours of  $^{12}\text{CO}$  emission integrated in the velocity ranges  $0.5\text{--}14.3 \text{ km s}^{-1}$  (blue) and  $23.8\text{--}39.7 \text{ km s}^{-1}$  (red) are shown. The direction of the outflow identified by Hull et al. (2014) ( $108^\circ$  E of N) is shown as a dotted line through MIR-b. Our proposed approximate directions of the outflow from MIR-c, and the blue wing of the outflow from MIR-a are shown as dotted lines through the respective sources. Magnetic field vectors are excluded for clarity. Panel (c) contours of ‘fast’  $^{12}\text{CO}$  emission, integrated in the ranges  $0.5\text{--}9.0 \text{ km s}^{-1}$  and  $28.0\text{--}36.5 \text{ km s}^{-1}$  are shown. Panel (d) contours of ‘slow’ emission, integrated in the ranges  $9.0\text{--}14.3$  and  $23.8\text{--}28.0 \text{ km s}^{-1}$  are shown. The CARMA beam is shown in each panel. The JCMT beam is shown in the top left-hand panel.

for hydrogen number densities  $n(\text{H}) > 300 \text{ cm}^{-3}$ . For our estimated gas density of  $n(\text{H}_2) \sim 3.0 \times 10^3 \text{ cm}^{-3}$  in the periphery of CB 54 ( $n(\text{H}) \sim 6.0 \times 10^3 \text{ cm}^{-3}$ ), this implies  $B_{\text{max}} = 69 \mu\text{G}$ . Our inferred upper limit,  $B < 27 \mu\text{G}$ , is below the more general Crutcher et al. (2010) upper limit at this gas density, and so is consistent with it, and also suggests that the magnetic field in the periphery of CB 54 is comparatively weak.

### 3.5 CARMA observations

The Yun & Clemens (1994) outflow emanates from the dense ridge at the centre of CB 54. Ciardi & Gómez Martín (2007) detected three Class 0 protostars in this ridge, MIR -a, -b and c, with masses of  $\sim 4 M_\odot$ ,  $\sim 1.5 M_\odot$  and  $> 0.2 M_\odot$ , respectively. This ridge was mapped in both 1.3-mm dust polarization and the  $^{12}\text{CO } J = 2 - 1$  transition (230.538 GHz) at  $3.64 \times 2.41 \text{ arcsec}^2$  resolution by Hull et al. (2014) using the CARMA (Combined Array for Research in Millimeter-wave Astronomy) interferometer as part of the TADPOL survey. We show the Hull et al. (2014) CARMA data in Fig. 6. The

magnetic field in the dense ridge in which the three protostars are forming appears to broadly lie along the length of the ridge (which itself is oriented  $\sim 145^\circ$  E of N, as shown in Fig. 6), and is similar to the magnetic field direction traced by POL-2 on larger scales in CB 54, and with the average field direction in the globule given by *Planck*. The magnetic field is approximately perpendicular to the ridge in the material to the north-east and south-west of the ridge, and parallel to the large-scale outflow direction, again consistent with the behaviour seen on larger scales in the POL-2 data. Histograms of POL-2 and CARMA magnetic field angles are shown in Fig. 7.

Inspection of the CARMA  $^{12}\text{CO}$  data presented by Hull et al. (2014) suggests that there is (i) a fast, highly collimated but quite faint outflow running  $\sim 45^\circ$  E of N, which appears most likely to be excited by MIR-c; (ii) a slower, broader, but brighter outflow running  $108^\circ$  E of N (identified by Hull et al. 2014), which appears to be excited by MIR-b; (iii) velocity structure suggestive of an outflow around MIR-a, the red wing of which is either not visible or not distinguishable from the MIR-b outflow, but the blue wing of which is oriented  $\sim 135^\circ$  E of N.

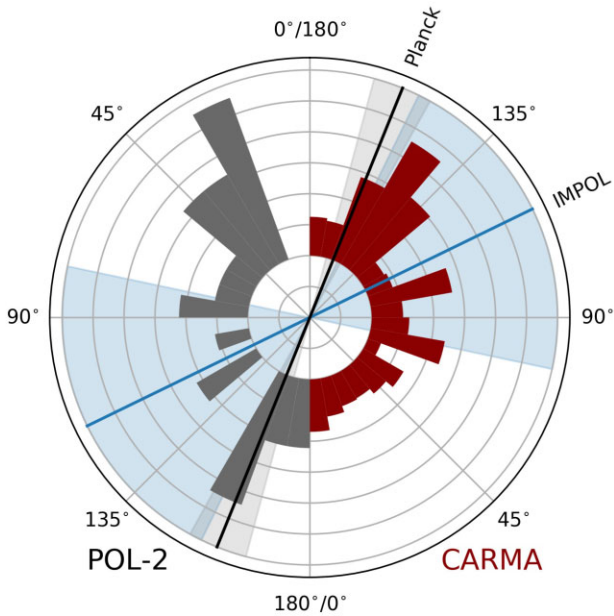


**Figure 7.** Circular histograms of POL-2 (grey) and CARMA (orange) magnetic field angles. Opposite angles agree, as described in the caption of Fig. 5. Mean *Planck* and *IMPOL* (Sen et al. 2005) magnetic field angles across CB 54 are shown, with their uncertainties shown as shaded sectors.

It appears from this that the large-scale CO outflow in CB 54 (Yun & Clemens 1994) is associated with the fast, collimated outflow which appears likely to arise from MIR-c. MIR-c is the faintest of the three Class 0 sources in the MIR, with a lower limit mass of  $>0.2 M_{\odot}$  (Ciardi & Gómez Martín 2007). This suggests that MIR-c is young and deeply embedded in the dense centre of CB 54.

The total mass in the large-scale outflow is  $\sim 4.7 M_{\odot}$  (Yun & Clemens 1994), significantly greater than the  $0.2 M_{\odot}$  lower limit placed on the mass of MIR-c itself by Ciardi & Gómez Martín (2007). Machida & Matsumoto (2012) suggest that in a single protostellar cloud core, 26–40 per cent of the initial cloud mass is incorporated into the protostar, while 8–49 per cent is ejected by the outflow. An outflow mass of  $4.7 M_{\odot}$  would thus imply a mass reservoir of  $9.6\text{--}58.8 M_{\odot}$  for MIR-c, and so an eventual mass of MIR-c of  $2.5\text{--}23.5 M_{\odot}$ . As there is no indication that CB 54 is a high-mass star-forming region, it seems likely that MIR-c is at the lower end of this potential mass range. As discussed above, the total mass of CB 54 appears to be broadly in the range  $\sim 60\text{--}120 M_{\odot}$ , sufficiently large to accommodate even the largest value of the implied mass reservoir for MIR-c, but is shared by the three forming protostars.

If MIR-c is indeed a young and deeply embedded Class 0 source, this suggests that the reshaping of the magnetic field by the CO outflow has been rapid, as does the dynamical time of the outflow,  $7 \times 10^4$  yr (Yun & Clemens 1994). The magnetic field direction implied by CARMA observations to the north-east and south-west of the dense ridge has a direction similar to that of the outflow emanating into these regions from MIR-c, and perpendicular to the average magnetic field direction in the dense ridge implied by both the POL-2 and CARMA observations. This supports the suggestion that this outflow is reshaping the magnetic field in the lower density material of the globule. Conversely, the magnetic field in the dense material of the ridge does not appear to be reordered by the MIR-c outflow.

## 4 DISCUSSION

If the outflow is indeed reshaping the magnetic field on large scales in the globule, this implies a relatively weak magnetic field in CB 54, significantly less than the likely maximum field strength of  $\sim 70 \mu\text{G}$  at this gas density implied by the Crutcher et al. (2010) relation. We here discuss the extent to which our observations support the suggestion that the magnetic field in CB 54 is dynamically subdominant. It is important to note that the relative dynamic importance of magnetic fields with respect to gravity, non-thermal motions and thermal pressure may differ. These energy balances are typically quantified using the mass-to-flux ratio, Alfvén Mach number, and plasma beta, respectively (e.g. Pattle et al. 2022, and refs. therein). The fact that stars have formed within CB 54 indicates that on at least some size scales, gravity must win out over the other forces involved in the evolution of the globule; however, simulations indicate that the energy balance on larger scales can make both a qualitative and quantitative difference to the evolution of star-forming regions (e.g. Seifried et al. 2020).

### 4.1 Density structure

The magnetic field geometry in CB 54 is well ordered and quite consistent in direction over many orders of magnitude in size scale, except in the vicinity of the Yun & Clemens (1994)/MIR-c outflow.

Strong-field star formation theory predicts that the minor axis of a dense core will lie parallel to the magnetic field direction (Mestel 1966; Basu, Ciolek & Wurster 2009). Basu (2000) shows that a magnetic field parallel to the minor axis of a triaxial core can have a wide range of orientations in projection, and is most likely to appear at an angle  $\sim 10^{\circ}\text{--}30^{\circ}$  to the projected minor axis of the core. We fitted a two-dimensional Gaussian model to the POL-2 I map of CB54, finding the best-fitting model to have a low aspect ratio of 1.15 (eccentricity  $e = 0.49$ ), and a major axis oriented  $118^{\circ}$  E of N. As discussed above, the mean magnetic field direction which we measure in the centre of CB 54 is  $163^{\circ} \pm 8^{\circ}$ . Thus, we infer that the magnetic field observed by POL-2 is offset from the minor axis of the globule by  $\sim 45^{\circ}$ , in projection.

However, performing the same-fitting process on the CARMA data are shown in Fig. 6 results in a best-fitting model with an aspect ratio of 1.56 ( $e = 0.77$ ), and a major axis oriented  $164^{\circ}$  E of N. The average magnetic field direction in the globule is thus very well-aligned with the major axis of the dense core in which the MIR-a, -b and -c protostars are forming. While this does not rule out the field being parallel to the minor axis in three dimensions, the probability of such a configuration is extremely low (Basu 2000). The similarity between the magnetic field angle measured by POL-2 and the major axis of the dense core, along with the (sub)millimetre brightness of this core, also suggests that the polarized emission observed by POL-2 may be dominated by unresolved emission from this dense core.

Many recent observations have shown that dense filaments preferentially align perpendicular to the direction of the local magnetic field, while lower density filaments tend to align parallel to the magnetic field (e.g. Alina et al. 2019; Soler 2019; Doi et al. 2020; Arzoumanian et al. 2021; Kwon et al. 2022). Simulations suggest that a transition from parallel to perpendicular alignment at high gas densities will typically only occur in clouds in which the magnetic field’s energetic importance is initially similar to or greater than that of gravity (e.g. Soler et al. 2013, 2020). Seifried et al. (2020) found that for their models with initial magnetic field strengths below  $\sim 5 \mu\text{G}$ , the magnetic field remained parallel or randomly oriented

with respect to both density and column density structures at all gas densities. However, there is no clear dependence of the transition density from parallel to perpendicular field/filament orientations on Alfvén Mach number (Pattle et al. 2022, and reference therein).

Whether the extended structure seen by CARMA in which the dense star-forming core at the centre of CB 54 is embedded can be considered as a ‘filament’ in the sense used in nearby molecular clouds (e.g. André et al. 2010) is arguable. The young protostars in CB 54 are none the less forming within a core which is embedded in a structure which is elongated parallel rather than perpendicular to the local plane-of-sky magnetic field direction. This would suggest a sub-dominant role for the magnetic field in comparison to gravity not only in the dense, star-forming core, but also in the evolution of the globule as a whole (e.g. Soler et al. 2013). It is, however, possible that the filament and the magnetic field could be perpendicular to one another in three dimensions despite being parallel in projection (e.g. Doi et al. 2020).

We note that an alternative explanation of the observed correlation between the outflow and magnetic field directions in the periphery of CB 54 is that the field geometry existed prior to the presence of the outflow, and that this field has shaped and channeled the outflow as it leaves the centre of the globule. However, this would require the field to have changed direction in the periphery of the globule when it is otherwise consistent in direction over many orders in magnitude in size scale. This scenario is difficult to physically motivate, but cannot be ruled out.

We also note that this apparent consistency of the magnetic field direction over several orders of magnitude in size scale suggests a highly ordered magnetic field (away from the outflow). The presence of such an ordered magnetic field suggests that non-thermal motions in the region are sub-Alfvénic (e.g. Ostriker et al. 2001). This implies a relatively strong magnetic field in CB 54 in comparison to turbulent motions. The magnetic field geometry which we observe in CB 54 thus allows us to hypothesize that in this region, while the dynamics are dominated by gravitational collapse, the magnetic energy in the region is greater than that of the non-thermal gas motions.

#### 4.2 Star formation efficiency

Both dynamically important magnetic fields and turbulence are expected to decrease SFE by providing support on large scales in molecular clouds (e.g. Price & Bate 2009; Federrath & Klessen 2013). If the magnetic field in CB 54 is indeed not sufficiently strong to support the globule against gravitational collapse, and turbulence in the globule is sub-Alfvénic, this suggests that gravitational collapse, and so star formation, in the globule ought to proceed relatively efficiently. The SFE of a molecular cloud varies from <1 per cent in regions of distributed star formation to up to ~40 per cent in regions forming large stellar clusters, with a mean value of ~15 per cent (Bonnell et al. 2011). Ciardi & Gómez Martín (2007) estimate a total mass of 10–15  $M_{\odot}$  for all of the sources embedded within CB 54, although as their estimated mass of MIR-c is a lower limit, so too is this total. Comparing this to our measured dust mass of  $117 \pm 7 M_{\odot}$  suggests a current SFE of  $M_{\text{embedded}}/(M_{\text{embedded}} + M_{\text{globule}}) \gtrsim 8\text{--}11$  per cent. As discussed above, the total mass of CB 54 is quite uncertain, but its centrally condensed geometry suggests that the mass which we estimate is representative of the total mass of the globule. The final SFE of CB 54 will be higher than this estimate, as star formation is still ongoing and the Class 0 protostars may yet accrete a significant fraction of their final mass from the globule (Andre, Ward-Thompson & Barsony 1993).

The current SFE of CB 54 appears to be lower than the mean efficiency of star-forming clouds (Bonnell et al. 2011). However, as discussed by Bonnell et al. (2011), comparison to this mean value can elide the significant differences between expected SFEs in high-mass and low-mass star-forming environments. Yun & Clemens (1990) inferred a typical SFE of ~6 per cent in Bok globules. Star formation in CB 54 thus appears to be proceeding somewhat more efficiently than in the average Bok globule.

More energetic outflows, and more efficient coupling between outflows and magnetic fields, are likely to result in lower SFE in molecular clouds as a whole (e.g. Krumholz & Federrath 2019). A total mass in the large-scale outflow from CB 54 of ~4.7  $M_{\odot}$  and a dynamical time of the outflow of  $\sim 7 \times 10^4$  yr (Yun & Clemens 1994) imply a very approximate mass outflow rate of  $\sim 7 \times 10^{-5} M_{\odot} \text{ yr}^{-1}$ . This is consistent with the typical outflow rate of  $\sim 10^{-4} M_{\odot} \text{ yr}^{-1}$  for young Class 0 sources (Bontemps et al. 1996), and with the expected  $\gtrsim 10^{-5} M_{\odot} \text{ yr}^{-1}$  mass accretion rate for Class 0 protostars (Whitworth & Ward-Thompson 2001), assuming that the mass accretion and outflow rates are comparable (e.g. Machida & Matsumoto 2012). This suggests that the large-scale CB 54 outflow is quite typical for an outflow being driven by a Class 0 source such as MIR-c. However, as the relationship between magnetic field strength and outflow rate is non-monotonic (Tomisaka 2002), and given its highly approximate nature, the outflow rate which we estimate should not be overinterpreted.

#### 4.3 Outflow orientations

Each of the three outflows in the centre of CB 54 has quite different orientation, as shown in Fig. 6. Random outflow alignments, with respect to both one another and to density structure, have been seen in both the Orion (Davis et al. 2009) and Perseus (Lee et al. 2016; Stephens et al. 2017) molecular clouds. However, Stephens et al. (2017) find that the distribution of outflow orientations in Perseus is also consistent with a mixture of parallel and perpendicular alignments with respect to density structure, with perpendicular alignment a factor of 3 more common than parallel. Conversely, Kong et al. (2019) find that in the IRDC G28.37 + 0.07 there is widespread alignment between outflow directions, with outflows having a strong preference to being perpendicular to the IRDC axis. A dynamically important magnetic field is likely to be a necessary condition for outflows to have a consistent orientation (Li, Klein & McKee 2018). However, random outflow directions could be created by interactions within multiple systems despite the presence of a strong magnetic field (Offner et al. 2016), and so the lack of a consistent outflow direction amongst the protostars in CB 54 is not necessarily indicative of a weak magnetic field in the region.

Ideal magnetohydrodynamic (MHD) simulations have shown that magnetic braking is more efficient in protostellar systems whose rotation axis is perpendicular to the magnetic field direction than in those whose rotation axis and magnetic field directions are parallel (Matsumoto & Tomisaka 2004; Hennebelle & Ciardi 2009). This efficient magnetic braking thus favours formation of a larger disc, and a weaker outflow, as misalignment between the field and rotation axes increases (Matsumoto & Tomisaka 2004). Creating a significant outflow in the highly misaligned case requires the system to have a high ratio of thermal kinetic to gravitational potential energy (Tsukamoto et al. 2018). Non-ideal MHD simulations can produce an outflow even in the fully misaligned case (Hirano et al. 2020), albeit a weak one.

The large-scale outflow from CB 54 appears to be significantly misaligned with the magnetic field direction in the core. While



we cannot determine the three-dimensional angle between the field and the outflow, the offset which we see in projection is near  $90^\circ$ . This extended outflow apparently perpendicular to the magnetic field direction appears to be unusual in the light of the predictions of both ideal and non-ideal simulations (Tsukamoto et al. 2018; Hirano et al. 2020), and so makes MIR-c a strong candidate for higher resolution interferometric follow-up, in order to determine whether its magnetic field direction on protostellar core scales is significantly offset from that in its surroundings.

#### 4.4 Comparison with other regions

Although we have not demonstrated a causal link between the outflow direction and the magnetic field geometry in the periphery of CB54, we note that if the outflow is indeed reshaping the magnetic field, this would be consistent both with previous observations of CB 54 (Bertrang et al. 2014) and with recent results from other regions, as well as with the predictions for the evolution of magnetic fields in the presence of outflows from numerical modelling (Hirano et al. 2020).

Magnetic fields have been seen to be reshaped by protostellar outflows on scales  $\sim 1000$  au ( $\sim 0.005$  pc) in recent ALMA observations of the BHR 71 IRS 2 source (Hull et al. 2020). In this case, the magnetic field traced by ALMA polarized dust emission appears to be that of the outflow cavity wall. However, the neighbouring IRS 1 source, which forms a wide binary with IRS 2, shows an apparently undistorted hourglass-shaped field. BHR 71 is  $\sim 40 M_\odot$  Bok globule at a distance of  $\sim 200$  pc, with a large-scale collimated outflow on size scales  $\sim 0.3$  pc (Bourke et al. 1997). Although lower mass, BHR 71 appears to be somewhat analogous to CB 54. However, Kandori et al. (2020) mapped the magnetic field in BHR 71 using SIRPOL NIR polarimetry at the IRSF, finding the field to be significantly distorted from the mean plane-of-sky field direction in the region. They ascribe this distortion to an interaction between the globule and a large-scale shock (cf. Inoue & Fukui 2013).

Davidson et al. (2011) observed the magnetic field structure on  $0.04$ – $0.09$  pc scales around the nearby low-mass B335, L1527, IC348-SMM2 protostars at  $350 \mu\text{m}$  using the SHARP polarimeter on the CSO. They found that the magnetic field geometries observed around L1527 and IC348-SMM2 could be consistent with magnetically regulated star formation models distorted by bipolar outflows, but that the magnetic field geometry around B335 was not consistent with magnetically regulated models, suggesting that a significant amount of distortion had occurred. They gave an outflow energy density of  $\sim 10^{-9}$  erg cm $^{-3}$  for B335, and further found that the energy densities of all of the outflows were sufficiently large to distort magnetic fields of strengths predicted by magnetically regulated star formation models. They suggested that the relative lack of distortion in L1527 and IC348-SMM2 is due to the youth of these outflows,  $\sim 10^3$  yr, compared to  $\sim 2 \times 10^4$  yr in B335. POL-2 and ALMA polarization observations of B335 support the presence of a field aligned with the outflow direction (Yen et al. 2019). The Davidson et al. (2011) sources are lower in mass than is CB 54, which houses multiple protostars. However, in both CB 54 and B335 a single outflow from a low-mass protostar appears to be shaping the magnetic field, suggesting an at least qualitative similarity between these sources.

In Orion B NGC 2071 (Lyo et al. 2021), the magnetic field appears to be shaped by the outflow from NGC 2071 IRS 3 on  $\sim 0.25$  pc scales, similar to CB 54. The NGC 2071 IRS 3 outflow, as estimated from  $^{13}\text{CO}$  emission, is significantly more energetic than the CB 54 outflow, with  $u_{\text{outflow}} = 2.33 \pm 0.32 \times 10^{-8}$  erg cm $^{-3}$  ( $\gtrsim 10^3 \times$  that of CB 54, as discussed above). Lyo et al. (2021) estimate a magnetic

field strength of  $563 \pm 421 \mu\text{G}$  in the central  $0.12$  pc of NGC 2071, and a magnetic energy density  $\sim 2 \times 10^{-8}$  erg cm $^{-3}$ , comparable to the outflow energy density in the region.

An extreme example of this behaviour is the explosive BN/KL outflow in the OMC-1 region of Orion A, which appears to have substantially reordered the magnetic field in the region on  $\sim 0.01$  pc scales (Cortes et al. 2021; see also Pattle et al. 2021a). However, the BN/KL outflow is an exceptional event, with an energy density of  $\sim 6 \times 10^{-4}$  erg cm $^{-3}$  over the area over which the magnetic field is reordered (Bally et al. 2017, 2020), more than three orders of magnitude greater than the magnetic energy density in the region (Cortes et al. 2021). Moreover, it is likely to have arisen from the interaction or decay of a multiple system, and so is not representative of usual conditions in star-forming cores.

The magnetic field geometry in dense star-forming cores is a key discriminant between weak- and strong-field modes of star formation (e.g. Myers & Basu 2021). Our observations of CB 54 suggest that even a weak outflow may be able to significantly alter the geometry of a weak magnetic field on scales  $\gtrsim 0.1$  pc in the cloud from which its driving protostar formed, and can do so on relatively short time-scales,  $\sim 10^4$  yr. This suggests that if we wish to understand the role of magnetic fields in the evolution of molecular clouds to gravitational instability, we must look at regions where stars have not yet formed. The magnetic field observed in the presence of an outflow-driving protostar cannot be relied upon to inform us of the field in the gas from which the protostar formed.

## 5 CONCLUSIONS

We have observed the large Bok globule CB 54 with the POL-2 polarimeter on the SCUBA-2 camera on the JCMT.

We find that the magnetic field in the centre of the globule is oriented  $163^\circ \pm 8^\circ$  E of N. The field in the periphery of the globule shows significant, ordered deviation from the mean field direction in the globule centre, with a mean orientation of  $63^\circ \pm 45^\circ$  and a median orientation of  $47^\circ$ . This deviation corresponds qualitatively with the contours of the extended but relatively weak  $^{12}\text{CO}$  outflow identified in the region by Yun & Clemens (1994), which appears to emanate from the Class 0 source MIR-c at the centre of the globule.

If the magnetic field in the periphery of the globule is indeed reshaped by the outflow, energetics analysis suggests that  $B < 27 \mu\text{G}$  in the area. This is less than the maximum likely value at this gas density,  $B_{\text{max}} \approx 69 \mu\text{G}$ , given by the Crutcher et al. (2010) relation.

Comparison with archival *Planck* and CARMA measurements shows that the field in the centre of the globule is consistent over several orders of magnitude in size scale, but oriented parallel to the density structure in the region in projection. This leads us to hypothesise that non-thermal motions in the region are sub-Alfvénic, but that the magnetic field itself is subdominant to gravity, suggesting that the gravitational collapse of CB 54 is relatively unimpeded. We estimate a star formation efficiency in CB 54 of  $\gtrsim 8$ – $11$  per cent. This is below the average value for molecular clouds, but may be relatively efficient for a Bok globule.

The outflow from CB 54 is extended despite significant misalignment between the outflow direction and the average magnetic field direction in the globule. This suggests that the likely driving source, the Class 0 protostar MIR-c, may be unusual, and merits high-resolution interferometric follow-up, to determine the magnetic field geometry in the protostellar envelope.

Our results suggest that even a weak outflow can significantly reshape weak magnetic fields in star-forming regions on scales  $> 0.1$  pc, and so that the magnetic field observed in a star-forming core

in the presence of outflows cannot be relied upon to inform us of the pre-star-formation magnetic conditions in the region.

## ACKNOWLEDGEMENTS

The authors would like to thank João Yun for helpful discussions of his observations of CB 54. KP is a Royal Society University Research Fellow supported by grant number URF\R1\211322, and in the early stages of this project was supported by the Ministry of Science and Technology of Taiwan under grant No. 106-2119-M-007-021-MY3. S-PL acknowledges grants from the Ministry of Science and Technology of Taiwan 106-2119-M-007-021-MY3 and 109-2112-M-007-010-MY3. SC acknowledges the SOFIA Science Center, operated by the Universities Space Research Association under contract NNA17BF53C with the National Aeronautics and Space Administration. S.W. and N.Z. acknowledge the support by the DLR/BMBF grant 50OR1910. WK was supported by the National Research Foundation of Korea (NRF) grant funded by the Korea government (MSIT) (NRF-2021R1F1A1061794). CWL is supported by the Basic Science Research Program through the National Research Foundation of Korea (NRF) funded by the Ministry of Education, Science and Technology (NRF-2019R1A2C1010851), and by the Korea Astronomy and Space Science Institute grant funded by the Korea government (MSIT) (Project No. 2022-1-840-05). The James Clerk Maxwell Telescope is operated by the East Asian Observatory on behalf of The National Astronomical Observatory of Japan; Academia Sinica Institute of Astronomy and Astrophysics; the Korea Astronomy and Space Science Institute; the National Astronomical Research Institute of Thailand; Center for Astronomical Mega-Science (as well as the National Key R&D Program of China with No. 2017YFA0402700). Additional funding support is provided by the Science and Technology Facilities Council of the United Kingdom and participating universities and organizations in the United Kingdom, Canada and Ireland. Additional funds for the construction of SCUBA-2 were provided by the Canada Foundation for Innovation. The authors wish to recognize and acknowledge the very significant cultural role and reverence that the summit of Maunakea has always had within the indigenous Hawaiian community. We are most fortunate to have the opportunity to conduct observations from this mountain.

## DATA AVAILABILITY

The raw data used in this analysis are available in the JCMT archive at the Canadian Astronomy Data Centre (CADC) under project codes M19AP016, M20AP022 and M21AP028. The reduced data presented in this paper are available from the CADC at <https://doi.org/10.11570/22.0020>.

## REFERENCES

Alina D., Ristorcelli I., Montier L., Abdikamalov E., Juvela M., Ferrière K., Bernard J. P., Micelotta E. R., 2019, *MNRAS*, 485, 2825  
 Andersson B. G., Lazarian A., Vaillancourt J. E., 2015, *ARA&A*, 53, 501  
 Andre P., Ward-Thompson D., Barsony M., 1993, *ApJ*, 406, 122  
 André P. et al., 2010, *A&A*, 518, L102  
 Arzoumanian D. et al., 2021, *A&A*, 647, A78  
 Bally J., 2016, *ARA&A*, 54, 491  
 Bally J., Ginsburg A., Arce H., Eisner J., Youngblood A., Zapata L., Zinnecker H., 2017, *ApJ*, 837, 60  
 Bally J., Ginsburg A., Forbrich J., Vargas-González J., 2020, *ApJ*, 889, 178  
 Basu S., 2000, *ApJ*, 540, L103  
 Basu S., Ciolek G. E., Wurster J., 2009, *New A*, 14, 221

Bertrang G., Wolf S., Das H. S., 2014, *A&A*, 565, A94  
 Bok B. J., Reilly E. F., 1947, *ApJ*, 105, 255  
 Bonnell I. A., Smith R. J., Clark P. C., Bate M. R., 2011, *MNRAS*, 410, 2339  
 Bontemps S., Andre P., Terebey S., Cabrit S., 1996, *A&A*, 311, 858  
 Bourke T. L. et al., 1997, *ApJ*, 476, 781  
 Brand J., Blitz L., 1993, *A&A*, 275, 67  
 Chandrasekhar S., Fermi E., 1953, *ApJ*, 118, 113  
 Chapin E. L., Berry D. S., Gibb A. G., Jenness T., Scott D., Tilanus R. P. J., Economou F., Holland W. S., 2013, *MNRAS*, 430, 2545  
 Ciardi D. R., Gómez Martín C., 2007, *ApJ*, 664, 377  
 Clemens D. P., Barvainis R., 1988, *ApJS*, 68, 257  
 Corradi R. L. M., Aznar R., Mampaso A., 1998, *MNRAS*, 297, 617  
 Cortes P. C. et al., 2021, *ApJ*, 907, 94  
 Coudé S. et al., 2016, *MNRAS*, 457, 2139  
 Crutcher R. M., 2012, *ARA&A*, 50, 29  
 Crutcher R. M., Wandelt B., Heiles C., Falgarone E., Troland T. H., 2010, *ApJ*, 725, 466  
 Davidson J. A. et al., 2011, *ApJ*, 732, 97  
 Davis L., 1951, *Phys. Rev.*, 81, 890  
 Davis C. J. et al., 2009, *A&A*, 496, 153  
 Doi Y. et al., 2020, *ApJ*, 899, 28  
 Drabek E. et al., 2012, *MNRAS*, 426, 23  
 Federrath C., Klessen R. S., 2013, *ApJ*, 763, 51  
 Friberg P., Bastien P., Berry D., Savini G., Graves S. F., Pattle K., 2016, in Holland W. S., Zmuidzinas J., eds, *SPIE Conf. Ser. Vol. 9914, Millimeter, Submillimeter, and Far-Infrared Detectors and Instrumentation for Astronomy VIII*. SPIE, Bellingham, p. 991403  
 Hennebelle P., Ciardi A., 2009, *A&A*, 506, L29  
 Henning T., Wolf S., Launhardt R., Waters R., 2001, *ApJ*, 561, 871  
 Hildebrand R. H., 1983, *QJRAS*, 24, 267  
 Hirano S., Tsukamoto Y., Basu S., Machida M. N., 2020, *ApJ*, 898, 118  
 Holland W. S. et al., 2013, *MNRAS*, 430, 2513  
 Hull C. L. H., Zhang Q., 2019, *Frontiers Astron. Space Sci.*, 6, 3  
 Hull C. L. H. et al., 2014, *ApJS*, 213, 13  
 Hull C. L. H., Le Gouellec V. J. M., Girart J. M., Tobin J. J., Bourke T. L., 2020, *ApJ*, 892, 152  
 Inoue T., Fukui Y., 2013, *ApJ*, 774, L31  
 Johnstone D. et al., 2017, *ApJ*, 836, 132  
 Juvela M., Harju J., Ysard N., Lunttila T., 2012, *A&A*, 538, A133  
 Kandori R. et al., 2020, *ApJ*, 892, 128  
 Kong S., Arce H. G., Maureira M. J., Caselli P., Tan J. C., Fontani F., 2019, *ApJ*, 874, 104  
 Krumholz M. R., Federrath C., 2019, *Frontiers Astron. Space Sci.*, 6, 7  
 Kwon W. et al., 2022, *ApJ*, 926, 163  
 Launhardt R., Henning T., 1997, *A&A*, 326, 329  
 Launhardt R. et al., 2010, *ApJS*, 188, 139  
 Lee K. I. et al., 2016, *ApJ*, 820, L2  
 Li P. S., Klein R. I., McKee C. F., 2018, *MNRAS*, 473, 4220  
 Lynds B. T., 1965, *ApJS*, 12, 163  
 Lyo A. R. et al., 2021, *ApJ*, 918, 85  
 Machida M. N., Matsumoto T., 2012, *MNRAS*, 421, 588  
 Mairs S. et al., 2021, *AJ*, 162, 191  
 Matsumoto T., Tomisaka K., 2004, *ApJ*, 616, 266  
 Matthews B. C., McPhee C. A., Fissel L. M., Curran R. L., 2009, *ApJS*, 182, 143  
 Mestel L., 1966, *MNRAS*, 133, 265  
 Montier L., Plaszczynski S., Levrier F., Tristram M., Alina D., Ristorcelli I., Bernard J. P., Guillet V., 2015, *A&A*, 574, A136  
 Myers P. C., Basu S., 2021, *ApJ*, 917, 35  
 Offner S. S. R., Chaban J., 2017, *ApJ*, 847, 104  
 Offner S. S. R., Dunham M. M., Lee K. I., Arce H. G., Fielding D. B., 2016, *ApJ*, 827, L11  
 Ossenkopf V., Henning T., 1994, *A&A*, 291, 943  
 Ostriker E. C., Stone J. M., Gammie C. F., 2001, *ApJ*, 546, 980  
 Pattle K. et al., 2015, *MNRAS*, 450, 1094  
 Pattle K. et al., 2021a, *MNRAS*, 503, 3414  
 Pattle K. et al., 2021b, *ApJ*, 907, 88

- Pattle K., Fissel L., Tahani M., Liu T., Ntormousi E., 2022, preprint (arXiv:2203.11179)
- Planck Collaboration XIX, 2015, *A&A*, 576, A104
- Planck Collaboration XLVIII, 2016, *A&A*, 596, A109
- Plaszczynski S., Montier L., Levrier F., Tristram M., 2014, *MNRAS*, 439, 4048
- Price D. J., Bate M. R., 2009, *MNRAS*, 398, 33
- Roy A. et al., 2014, *A&A*, 562, A138
- Seifried D., Walch S., Weis M., Reissl S., Soler J. D., Klessen R. S., Joshi P. R., 2020, *MNRAS*, 497, 4196
- Sen A. K., Mukai T., Gupta R., Das H. S., 2005, *MNRAS*, 361, 177
- Sen A. K., Il'in V. B., Prokopjeva M. S., Gupta R., 2021, *MNRAS*, 503, 5274
- Septúlveda I., Anglada G., Estalella R., López R., Girart J. M., Yang J., 2011, *A&A*, 527, A41
- Serkowski K., 1962, *Adv. Astron. Astrophys.*, 1, 289
- Soler J. D., 2019, *A&A*, 629, A96
- Soler J. D., Hennebelle P., Martin P. G., Miville-Deschênes M. A., Netterfield C. B., Fissel L. M., 2013, *ApJ*, 774, 128
- Stephens I. W. et al., 2017, *ApJ*, 846, 16
- Tomisaka K., 2002, *ApJ*, 575, 306
- Tsukamoto Y., Okuzumi S., Iwasaki K., Machida M. N., Inutsuka S., 2018, *ApJ*, 868, 22
- Whitworth A. P., Ward-Thompson D., 2001, *ApJ*, 547, 317
- Wolf S., Launhardt R., Henning T., 2003, *ApJ*, 592, 233
- Yen H.-W. et al., 2019, *ApJ*, 871, 243
- Yen H.-W. et al., 2021, *ApJ*, 907, 33
- Yun J. L., 1996, *AJ*, 111, 930
- Yun J. L., Clemens D. P., 1990, *ApJ*, 365, L73
- Yun J. L., Clemens D. P., 1994, *ApJS*, 92, 145

## APPENDIX A: STOKES MAPS

In this appendix, we present maps of Stokes  $Q$  (Fig. A1) and  $U$  (Fig. A2) emission, and of non-debiased polarized intensity  $PI'$  (Fig. A3), on 8-arcsec pixels.

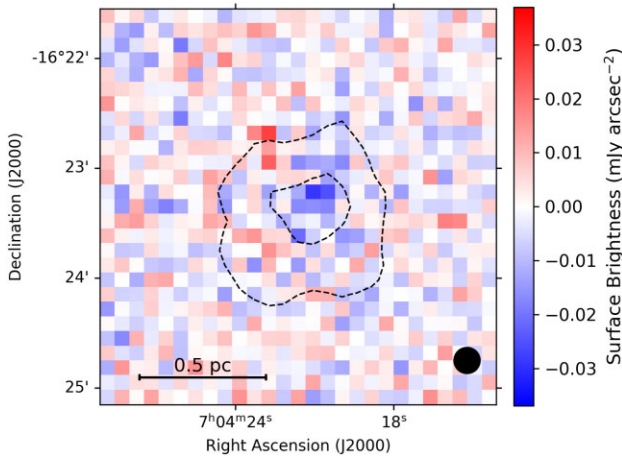


**Figure A1.** Stokes  $Q$  emission in CB 54, shown on 8-arcsec pixels. Contours show Stokes  $I$  emission, marking 2 and 20 per cent of the maximum Stokes  $I$  value in the globule.

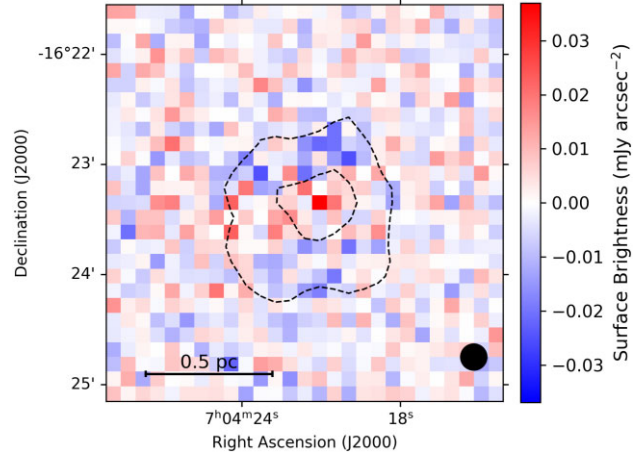


**Figure A2.** Stokes  $U$  emission in CB 54, shown on 8-arcsec pixels. Contours show Stokes  $I$  emission, marking 2 and 20 per cent of the maximum Stokes  $I$  value in the globule.

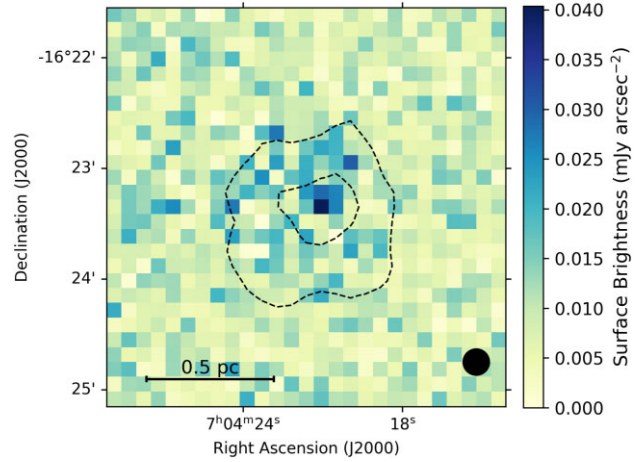


**Figure A3.** Non-debiased polarized intensity  $PI'$  emission in CB 54, shown on 8-arcsec pixels. Contours show Stokes  $I$  emission, marking 2 and 20 per cent of the maximum Stokes  $I$  value in the globule.

This paper has been typeset from a  $\text{\TeX}/\text{\LaTeX}$  file prepared by the author.